Numerical Analysis of Yawed Turbine Wake under Atmospheric Boundary Layer Flows

Xu Ning, Decheng Wan*

State Key Laboratory of Ocean Engineering, School of Naval Architecture, Ocean and Civil Engineering, Shanghai Jiao Tong University, Collaborative Innovation Center for Advanced Ship and Deep-Sea Exploration, Shanghai 200240, China

*Corresponding author: dcwan@sjtu.edu.cn

Abstract

Yaw is the most common working condition of a wind turbine and the key of reducing the fatigue loads and improving the performance of a wind farm is to understand the wake characteristics of a wind turbine in yaw condition. A neutral boundary layer flow in the atmosphere is simulated by the LES technique using the solver developed based on OpenFOAM and the wake flow of a yawed wind turbine modeled by the actuator line is studied. The time-average velocity field proves the practicability of the yaw control operation in optimizing the total power output of a wind farm, but from the cross section contours, the velocity distribution in the wake of a yawed turbine is not completely symmetric and the vertical wake deflection cannot be neglected, which is the main source of errors of the analytical wake models based on the gaussian distribution assumption. The time history curves and frequency spectrum of the wake meandering gained from the filtered flow data indicate that the yaw conditions have limited impacts on the wake meandering and the downstream position x is the main factor that affects the lateral movement of the wake. As the wake moves downstream, the meandering intensity increases and two distinct dominant frequencies of the wiggling wake are found in the far wake, of which the Strouhal numbers are 0.09 and between 0.1 ~ 0.3 respectively.

Keywords: Yawed wind turbine; Atmospheric boundary layer; Large eddy simulation; Wake meandering

Introduction

A wind turbine works in yaw condition when the turbine rotor is not perpendicular to the incoming wind, which is in fact the most frequent working condition in a real wind farm. The inevitable misalignment between the horizontal axis of the wind turbine and the wind speed vector could, to a certain degree, reduce the aerodynamic performance and influence the development of the wake flow[1]. However, instead of aligning all the wind turbines perfectly with the wind direction, appropriate active yaw operation of the wind turbines located upstream will significantly decrease the production loss of downstream wind turbines caused by the turbine wake and thus achieve the overall optimal performance of the wind farm[2][3]. To build up a control algorithm that computes the optimal yaw angle of each turbine given the wind regime and the layout of the wind farm, a systematic study of the wake characteristics of a yawed wind turbine under various inflow conditions is necessary.

Grant et al.[4] conducted the very early wind-tunnel experiments to observe the vortex structure and the deflection phenomenon in the near wake region of a yawed model turbine. Similar experimental studies focusing on the near wake flow of wind turbine in yaw condition were also performed by Haans et al.[5] and Krogstad & Adaramola[6], with the later work revealing that the power output of a yawed wind turbine is proportional to $\cos^3\gamma$ (γ is the yaw angle).

Bartl et al.[7] used Laser Doppler anemometry in the experiment to investigate the influence of the inflow shear and turbulence intensity on the evolution of the deflected wake. Bastankhah and Porté-Agel[8]-[10] performed a series of experimental and theoretical researches on both the near and far wake flow structure and dynamics of yawed wind turbines and integrated the yaw operation into the optimization algorithm of the wind farm. Moreover, the CFD technique also plays significant role in related studies. Jiménez et al.[11] introduced the body force computed by the actuator disk model to the LES equations for incompressible flow to simulate the wake deflection and trajectories and the results agreed well with the experimental measurements as well as the prediction of an analytical model. Also from LES case studies, which consider the different atmospheric stabilities and the uncertainties of wake defection, Vollmer et al.[12] emphasized the importance of the accurate measurement of the shear and turbulence of incoming flow in the prediction of the downstream wake position and indicated that the active yaw operation could effectively improve the performance of the wind farm in condition of an atmosphere with relatively high stability. Based on the work of Bastankhah and Porté-Agel[9], Guo-Wei Qian and Takeshi Ishihara[13] proposed an improved analytical wake model for yawed wind turbines able to predict both velocity deficit and turbulence intensity, of which the results showed good agreements with those of the RANS simulation cases.

The work mentioned above mainly concentrate on the time averaged characteristics of the turbine wake, aiming to precisely predict the velocity and turbulence of the wake downstream. However, under atmospheric ambient flow, the extension and expansion of the wake is not subject to a mathematically expressible rule at a certain instant. The stochastic behavior of turbine wake, meandering for example, has noticeable influence on the performance of downstream wind turbines. Therefore, in the present work the wake of yawed wind turbine under neutral boundary layer flow is simulated and the features of wake meandering as well as the time averaged flow field are studied.

Numerical Method

Governing Equations

Considering the superiority in simulating the unsteady large scale turbulent structures in the atmospheric flow, large eddy simulation technique is introduced in the present study. In order to simulate the ubiquitous effects of the earth's rotation and the buoyance caused by the spatial difference of temperature, the incompressible Navier-Stokes equation consists additionally of a Coriolis term and a buoyancy term, which, together with the continuity equation, constitutes the governing equation set as follows:

$$\frac{\partial \overline{u_i}}{\partial x_i} = 0 \tag{1}$$

$$\frac{\partial \overline{u_i}}{\partial t} + \frac{\partial}{\partial x_j}(\overline{u_j}\,\overline{u_i}) = \underbrace{-2\varepsilon_{i3k}\Omega_3\overline{u_k}}_{\text{I}} \underbrace{-\frac{1}{\rho}\frac{\partial}{\partial x_i}p_0(x,y)}_{\text{II}} \underbrace{-\frac{\partial \tilde{p}}{\partial x_i}}_{\text{III}} \underbrace{-\frac{\partial \tau_{ij}^D}{\partial x_j}}_{\text{IV}} \underbrace{+g\left(\frac{\overline{\theta}-\theta_0}{\theta_0}\right)\delta_{i3}}_{\text{V}} \underbrace{+\frac{1}{\rho}f_i}_{\text{VI}} \tag{2}$$

The Coriolis force is computed by term I, where ε_{ijk} is the alternating tensor and $\Omega = \omega[0, \cos(\phi), \sin(\phi)]$ (the planetary rotation rate $\omega = 7.27\times10^{-5} rad/s$) is the rotation rate vector. The gradient of resolved-scale pressure $\overline{p}$ is divided into term II, the background pressure gradient, and term III, which consists of the gradient of one third of the stress tensor trace $\tau_{kk}/3$ and $\hat{p} = \overline{p} - p_0(x,y) + \rho_0 gz$. τ_{ij} is the fluid stress tensor and in term

$\tau_{ij}^D = \tau_{ij} - \delta_{ij}\tau_{kk}/3$, where δ_{ij} is the Kronecker delta. The Smargorinsky eddy viscosity model is used to deal with the τ_{ij}^D in term :

$$\tau_{ij}^D = -2\upsilon^{SFS}\overline{S_{ij}} \tag{3}$$

$$\overline{S_{ij}} = \frac{1}{2}\left(\frac{\partial \overline{u_i}}{\partial x_j} + \frac{\partial \overline{u_j}}{\partial x_i}\right) \tag{4}$$

Where the sub-filter scale viscosity $\upsilon^{SFS} = (C_s\Delta)^2(\overline{S_{ij}}\,\overline{S_{ij}})^{1/2}$, C_s is a constant, set to 0.14 in this work. The density ρ is considered uniform in the whole domain, so the buoyancy effect has to be modeled by the Boussinesq approximation as shown in term V, where $\overline{\theta}$ and $\theta_0 = 300K$ represent the resolved scale potential temperature and reference potential temperature respectively. A temperature transport equation decoupled from the N-S equation needs to solved to obtain the potential temperature field:

$$\frac{\partial \overline{\theta}}{\partial t} + \frac{\partial}{\partial x_j}(u_j\overline{\theta}) = -\frac{\partial q_j}{\partial x_j} \tag{5}$$

$$q_j = -\frac{\upsilon^{SFS}}{\mathrm{Pr}_t}\frac{\partial \overline{\theta}}{\partial x_j} \tag{6}$$

Equation (6) models the molecular and sub-filter effects in the temperature diffusion, where the turbulent Prandtl number $\mathrm{Pr}_t = 1/3$. Term VI represents the aerodynamic force of the wind turbine blades exerted to the flow field, which is modeled by the actuator line model presented in the next part.

Actuator Line Model

First proposed by Sørensen and Shen[14], the actuator line model is widely used in the researches of wind turbine aerodynamics. The main idea is to directly exert the equivalent aerodynamic force to the flow field instead of building up the physical model of the turbine blades. Concretely, the blade is firstly divided into tens of airfoil segments and of each the lift force and drag force generated is expressed as:

$$L = \frac{1}{2}C_l\rho U_{rel}^2 c\,dr \tag{7}$$

$$D = \frac{1}{2}C_d\rho U_{rel}^2 c\,dr \tag{8}$$

Where C_l and C_d are lift and drag coefficients as function of the attack angle α, c the chord length and dr the width of a airfoil segment. The relative velocity of a certain blade segment is computed as:

$$U_{rel} = \sqrt{U_x^2 + (\Omega r - U_\theta)^2} \tag{9}$$

U_x, U_θ and Ω are axial velocity, tangential velocity and rotation speed of the rotor respectively, among which the relationship is depicted in Fig. 1. The vector sum of the lift force and drag force f is considered equal to the aerodynamic force generated by the corresponding airfoil segment. Before applying f to the flow field, it is necessary to redistribute and smooth the concentrated force from one point to a ball-shaped region to avoid the possible numerical divergence. As following, the projection is implemented by taking the convolution of f and the regularization kernel η_ε :

$$f_\varepsilon = f \otimes \eta_\varepsilon \quad , \quad \eta_\varepsilon(d) = \frac{1}{\varepsilon^2 \pi^{3/2}} \exp\left[-\left(\frac{d}{\varepsilon} \right)^2 \right] \tag{10}$$

Where d represents the distance between the grid points and a certain actuator point and ε is a constant that controls the concentration of the aerodynamic force.

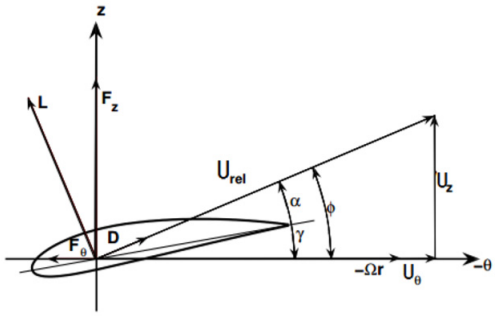

Figure 1. Velocity vector in the cross section of an airfoil segment

Simulation Setup

Computation Domain

Basically, there are two methodologies to realize the atmospheric boundary layer inflow condition: (i) directly producing the pseudo atmospheric boundary layer inflow in the inlet plane through mathematical model based on the spectral tensor model[15] or synthetic harmonic waves[16]; (ii) simulating a fully developed boundary layer flow in a precursor case and collecting the flow data in the cross sections as the inflow condition in the successor case. In the present work, the latter is adopted because the synthetic turbulent energy cannot avoid decay as flowing downstream since no energy is generated to compensate the dissipation[17]. In order to simulate the divers scale turbulent structures in the atmosphere, which could range from a few millimeters to more than a kilometer, the width and height of the precursor domain should be large enough. Therefore, both the width and height are set to 1008m and the length is set to 2016m, so as to investigate the flow in far wake region. The layout and main dimensions of the domain are indicated in Fig. 2.

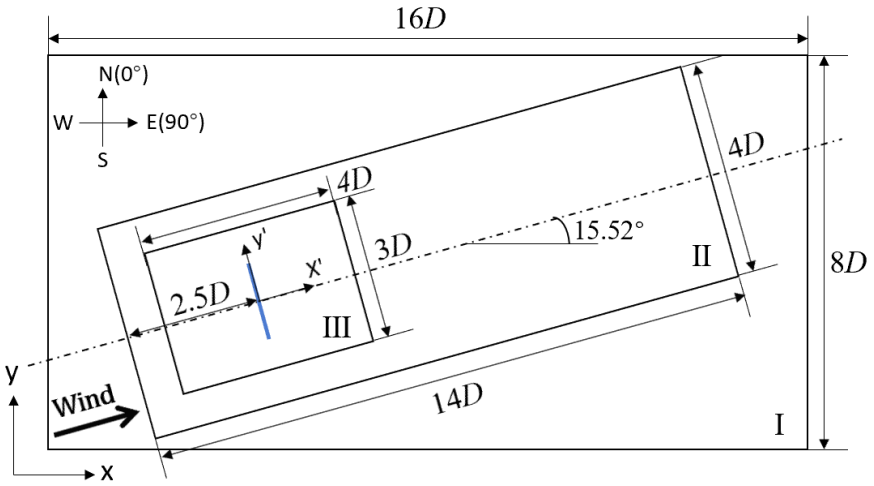

Figure 2. Layout and main dimensions of the computation domain

The unit grid scale in the background mesh $\Delta_I = 8m$ and in the region II that covers the vicinity

of the wind turbine and the whole wake region, the side length of every single mesh cell Δ_{II} is set to 4m. Region III with the finest mesh resolution $\Delta_{III} = 2m$ includes the turbine rotor and its vicinity so that the wind turbine aerodynamics and the vortex structure induced behind the blade tip and root can be simulated correctly. For analyzing the wake data more conveniently, a new coordinate system is created and used in the following work, with the original point located at the position of the wind turbine tower and the x-y plane rotating 15.52° around the z axis in anticlockwise direction to align the x axis with wind direction. This coordinate system is also shown in Fig. 2.

Boundary Conditions and Case Setup

For the precursor case, all four vertical planes of the domain is set to cycle boundary condition, allowing the boundary flow to fully develop within a finit computation domain. The free-slip condition is applied to the top, meaning no friction and flux at this plane. Considering the real ground is not smooth but with a rough surface which cannot be directly simulated, a wall model proposed by Moeng[18] with the roughness length set to 0.001, is introduced to approximate the flow near the ground. The mean wind direction is at an angle of 15.52° to the original x-axis and the wind speed at the hub height is prescribed to the rated wind speed of the NREL-5MW wind turbine $11.4m/s$. The computation runs with a time step of $0.5s$ until the boundary layer flow reached quasi-equilibrium state under the horizontal driving pressure. Then the simulation continues but with the time step reset to $0.02s$ and the flow data is collected as the inflow database of the successor cases.

Table 1: Main parameters of the NREL-5MW wind turbine

	Values	Units
Rating	5.00	MW
Rotor orientation	Upwind	–
Blade number	3	–
Rotor diameter	126	m
Hub height	90	m
Rated wind speed	11.4	m/s
Rated rotation speed	12.1	rpm

Three successor cases were set up, among which the first case contains a wind turbine rotating at $12.1rpm$ with its rotor directly facing the wind direction and in the other two cases, the wind turbine is 30° yawed in clockwise and counterclockwise direction respectively while keeping the other conditions unchanged. The main object is to investigate the wake deflection and wake meandering phenomenon in the far wake region of the yawed wind turbine under neutral boundary layer flow through a comparative study with the non-yaw condition case. The main properties of the wind turbine is listed in Table 1.

Results

NBL Flow Validation

The boundary layer flow is considered fully developed after the simulation of $18000s$, with the wind speed and direction at the hub height stable at the prescribed values. Fig. 4 shows the time averaged vertical profiles of streamwise wind speed, wind direction and the streamwise

turbulent intensity which is defined as the following formula:

$$I_x(z) = \frac{\sqrt{\overline{u'u'}(z)}}{\overline{u}(z)} = \frac{\sigma_u}{u_0(z)} \tag{10}$$

Where the overbar represents time averaging, $u' = u(t) - \overline{u}$, and $u_0 = \overline{u}$ is considered as the ambient flow velocity in streamwise direction. In order to validate the velocity profile, the logarithmic law is also plotted in Fig. 3(a) and the measured velocity in the Prandtl layer accords well with the theoretical value. The three red dash lines in the picture mark the top, bottom and the hub height of the turbine rotor. Strong wind shear occurs around the hub height and the speed difference between the wind speeds at top and bottom of the rotor attains $1.68m/s$, which is a typical characteristic of the neutral boundary layer flow. As shown in Fig. 3(b), under the Coriolis effect, the wind turbine also experiences a wind direction shear of two degree. The influence of wind direction shear on the development of the wake cannot be neglected, because a deviation of 2° across the rotor will stretch the wake transversely by $0.18D \sim 0.28D$ after the advection of $5D \sim 8D$, which is the normal streamwise spacing between two wind turbines in a wind farm. From the Fig.3(c), the streamwise turbulent intensity near the ground reaches 10% and decreases rapidly as the height rises to $200m$, indicating that properly raising the hub height of the wind turbine could significantly reduce the fatigue loads on the blades. The turbulent intensity at the hub height in the precursor case is 6.4%, a typical value of the ABL flow over a calm sea or an empty ground, which corresponds to the roughness length of 0.001 prescribed in the wall model.

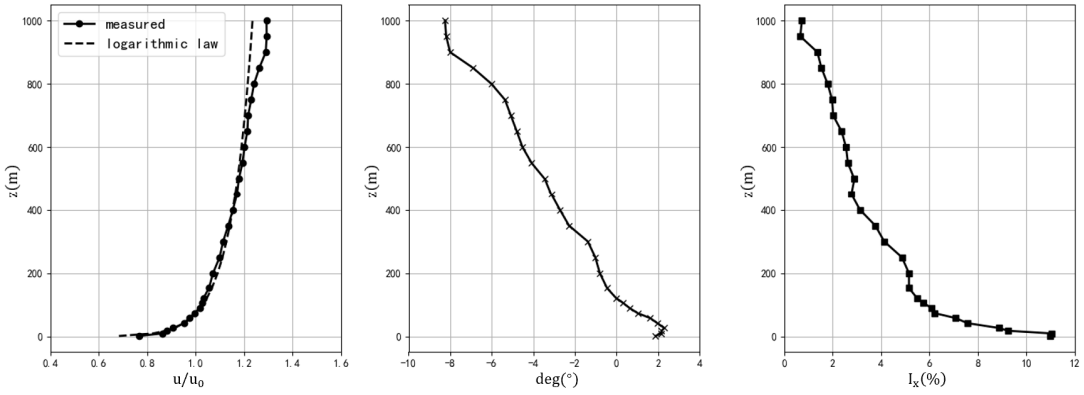

(a) (b) (c)

Figure 3. Time averaged characteristics of the atmospheric boundary layer flow in precursor case: (a)streamwise wind speed profile; (b)wind direction profile; (c)streamwise turbulent intensity profile

Velocity Deficit and Wake Deflection

The velocity deficit represents the loss of the streamwise wind speed in the wake region normalized by the ambient inflow velocity, as defined by the following expression:

$$u_d = 1 - u/u_0 \tag{10}$$

The velocity deficit distributions in different downstream positions in the central vertical plane and the hub height horizontal plane are plotted in Fig. 4, with the origin of height set to hub height and the scale normalized by rotor radius R. As seen in Fig. 4(a), the velocity deficit profiles of the non-yawed turbine show symmetry until $6D$ downstream, after which the wind speed in the upper part of the wake region recovers faster than that of the lower part, because

the expansion of the wake is blocked by the ground and the compensation of the kinetic energy is mainly acquired through the shear layer turbulent flow in the top part of the wake. The velocity deficit in the wake of a yawed turbine is relatively small compared with that of a non-yawed turbine, because only the velocity component perpendicular to the rotor plane can be utilized. Moreover, the crosswise thrust induced by the misalignment between the turbine shaft and wind direction push the whole wake aside. For this reason, the flow data probed in the central longitudinal plane of the domain shown in Fig. 4(a) show very low level velocity deficit in the far downstream positions, which indicates a low power loss of downstream wind turbines and demonstrates the practicability of yaw operation in the wind farm optimization algorithm. From Fig. 4(b), the wake center in yaw condition deflects aside as moving downstream, with the lateral displacement reaching $1R$ in $10D$ position, and it is clearly seen in all cases that the velocity deficit curves transform from M shape in the near wake to gaussian curves after $x = 4D$. This self-similarity feature in the far wake is also one of the basic assumptions in the analytical models of wind turbine wake.

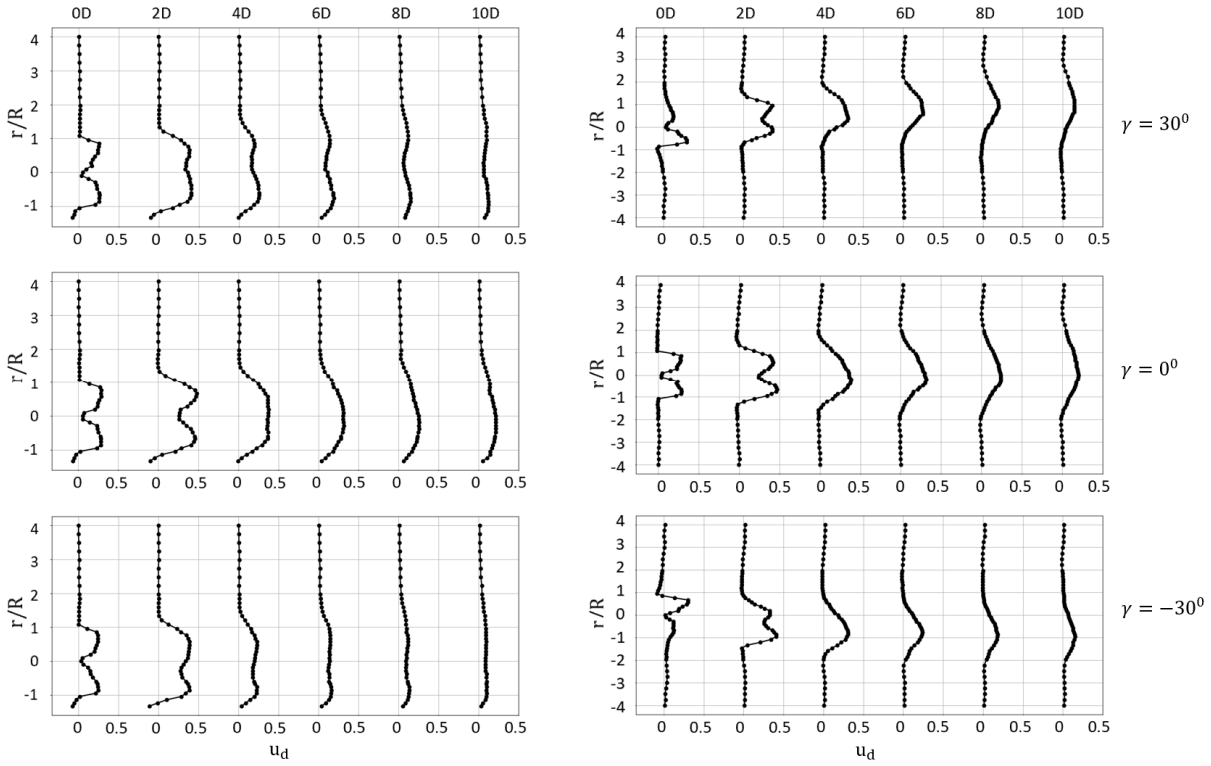

Figure 4. Time averaged velocity deficit in different downstream positions: (a)central longitudinal plane; (b) hub height horizontal plane

Fig. 5(a) shows the time averaged velocity deficit contours in the hub height horizontal plane of case 1~3. The profile in every x position is fitted by a gaussian curve, of which the parameter μ indicates the coordinate of the wake center and plotted as black dotted line in this figure. The velocity deficit in the near wake in case 0 is much more serious than those in the other two cases and due to the larger wake width, it takes longer distance for the shear layer to fully develop and recover the wind speed around the wake center. By contrast, the effective area against the wind reduces when a turbine yaws, so the wake region narrows and the shear layers in both sides meet earlier with each other in the wake core region. Moreover, the wake deflection of the yawed turbine is also clearly seen and the time averaged wake traces of the two turbines yawed in opposite direction show symmetry in lateral displacement. The wake

skew angle ($\theta \approx \tan\theta = u/v$) reveals the tendency of the lateral movement of the wake. From the wake skew angle contour in Fig. 5(b), in case 0, the outwards radial flow induced by the turbine blades weakens immediately behind the rotor, while in cases with yawed turbines, the windward part of the rotor induces the air to flow inward and this tendency becomes even more strong downstream in the near wake, dominating the whole wake region and gradually decreasing in the far wake region.

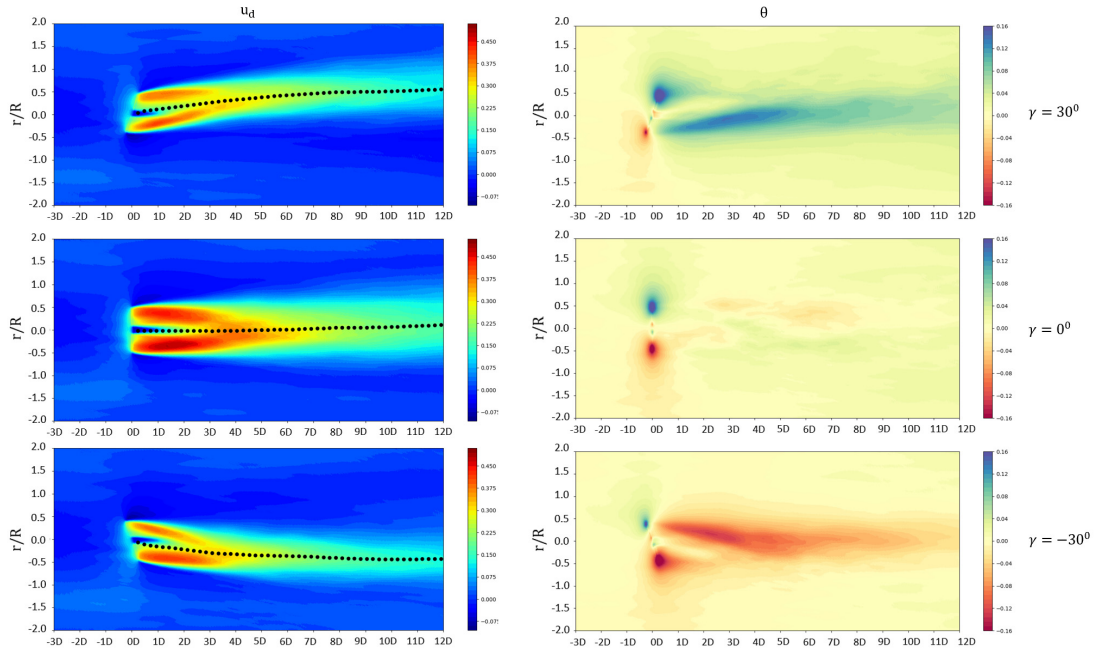

Figure 5. Contours of time averaged wake field in the hub height horizontal plane: (a) velocity deficit; (b) wake skew angle

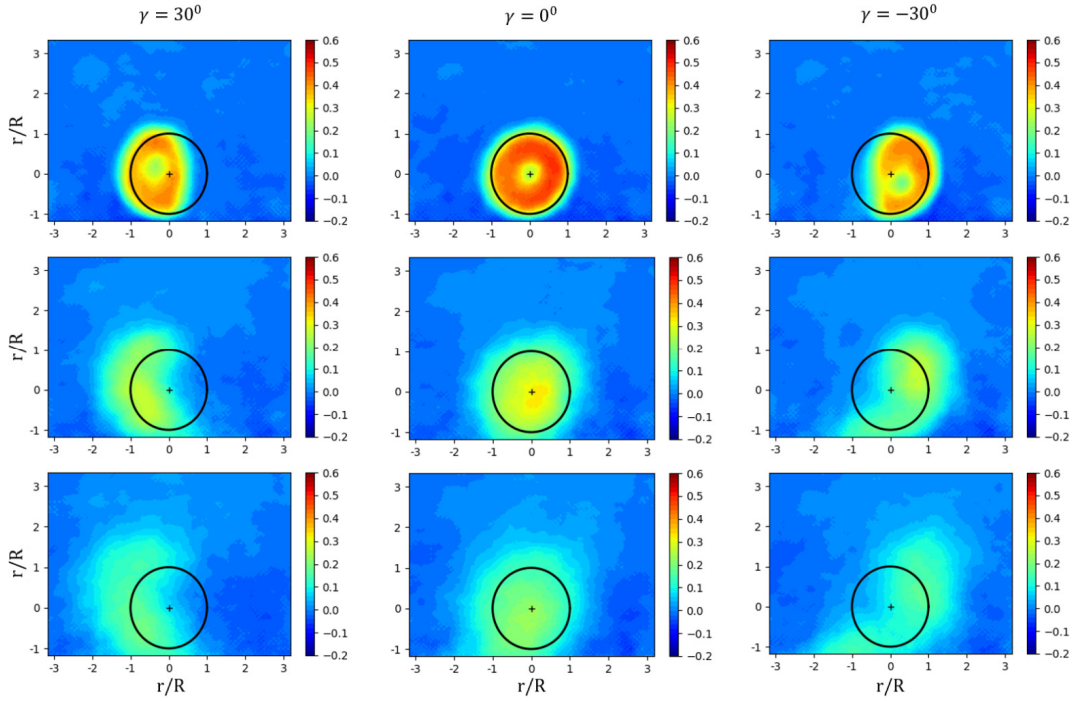

Figure 6. Contours of time averaged velocity deficit in different cross sections

To illustrate the wake deflection in both y and z direction, the contours of time averaged velocity deficit of $x = 2D,\ 6D,\ 10D$ cross sections are shown in Fig. 6, with the hub center marked by a plus sign and the rotor edge marked by a black circle. For $x = 2D$ position, the wakes in case 1 and 2, compared with the round wake region in case 0, show the shape of a ellipse and the wake center of the turbine with $\gamma = 30°$ moves upward and the other moves downward. In $6D$ downwind location, the wake changes into kidney-shape, caused by the forming of a counter-rotating vortex pair in the far wake region of a turbine with high yaw angle[8] and the wake remain this cross section shape until $x = 10D$. Furthermore, the two wakes of turbines yawed in opposite directions are not completely symmetric and the vertical deflection of the wake center seems to have the same order of the magnitude as the lateral. Thus the yaw direction and the vertical wake deflection cannot be neglected when predicting and describing the wake flow of a turbine in yaw condition.

Wake Meandering

As seen in the Fig. 7, which shows the instantaneous velocity deficit field in the hub height plane, The trace of the wake center of an instant marked by the solid line is not a smooth line, but wiggles around the average center line. This phenomenon called wake meandering is caused by the large-scale turbulent structure in the atmosphere and the meandering is not completely random but demonstrates certain statistical properties. It should be noted that the velocity data used in this part are all filtered temporally with a τ-window:

$$\hat{u} = \frac{1}{\tau}\int_{t-\tau/2}^{t+\tau/2} u(t)dt,\ \ \tau\text{=3s} \tag{11}$$

The purpose is to conserve the large scale flow structure and eliminate the high frequent turbulence, which could lead to the bias in the estimation of the wake meandering. The value $\tau = 0.6T \approx 3s$ is chosen as same as the window width used by Foti[19].

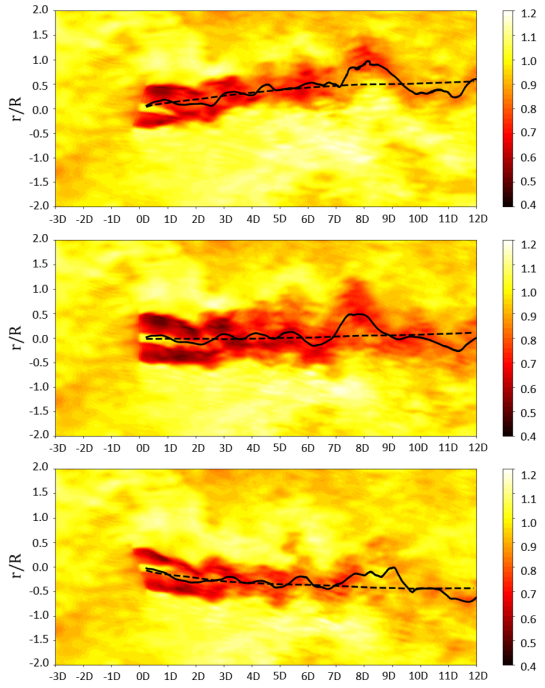

Figure 7. Filtered velocity deficit field in hub height plane of $t = 380s$

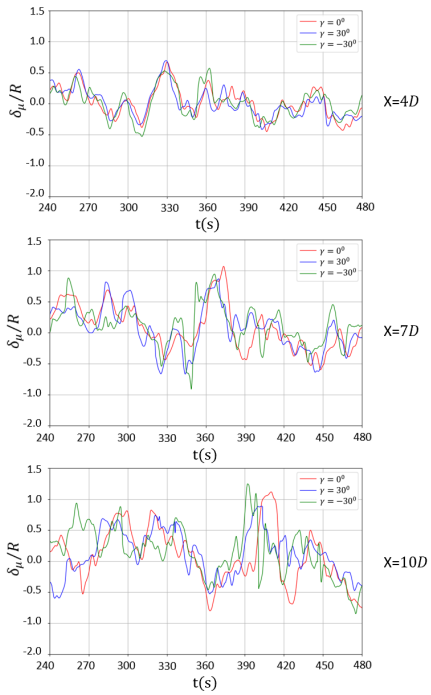

Figure 8. Time history curves of δ_μ in different downstream positions

The Fig. 7 shows that the levels of the wake meandering in all three cases are nearly the same, although the velocity deficit in case 0 is larger than those in yaw condition, and the amplitudes of the wiggle increases as it moves downstream. The lateral displacement of an instantaneous wake center relative to its average value in a certain downstream position, defined as $\delta_\mu(t) = \mu(t) - \bar{\mu}(t)$ is used to describe the scale of the wake meandering. Because $4D \sim 10D$ is the common streamwise spacing between turbines in the wind farm, the study of the wake meandering in this range has more reference value for the engineering practice. The $\delta_\mu(t)$ in the $x = 4D,\ 7D,\ 10D$ locations are acquired by fitting the gaussian curve to the temporally filtered velocity deficit profile of the three positions and the time history curves of $\delta_\mu(t)$ normalized by rotor radii R for case 1~3 are plotted in Fig. 8. The results show that there is strong correlation between the curves for the same position of three cases. Considering the inflow data of case 1~3 are exactly the same (collected from the same precursor case), the similarity of the time history meandering curves of different cases provides the strong evidence for the assumption made by Larsen et al. in his work[20], which indicates that the wake acts as a passive tracer driven by the large-scale turbulence structures in the atmospheric boundary layer.

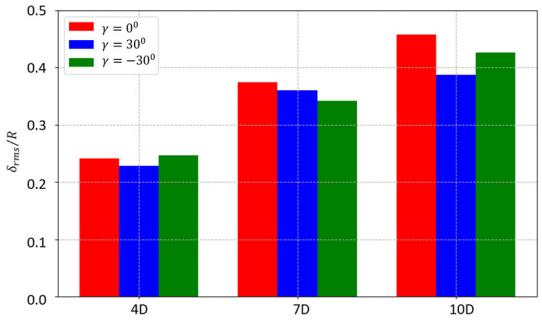

Figure 9. Root mean square of δ_μ

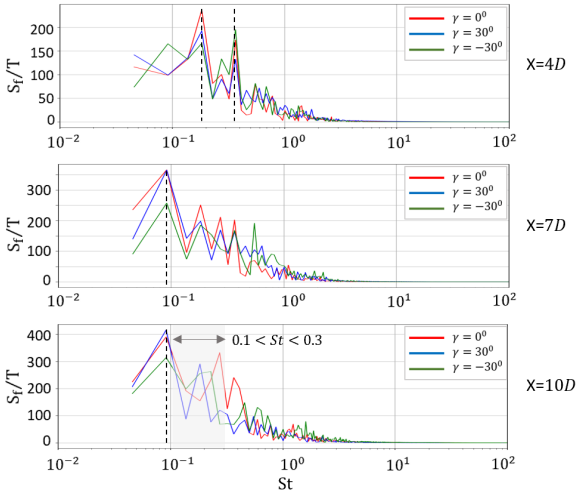

Figure 10. Frequency spectrum of δ_μ

To investigate the influence of yaw condition and downstream distance on the intensity of the wake meandering, the root mean square of $\delta_\mu(t)$ is computed with the results shown in Fig. 9. Apparently the wake meandering intensity raises as the wake moves downstream, which is also demonstrated in Fig. 7 and 8. Moreover, by comparison, the influence of yaw condition on the wake meandering intensity is inappreciable, because the difference of rms among three cases is less than $0.05R$, which can be neglected in the performance prediction of a wind farm. The normalized frequency spectrums gained by the FFT of $\delta_\mu(t)$ series are depicted in Fig. 10. The spectrum for $x = 4D$ shows two distinct peaks corresponding to $St = 0.18$ and $St = 0.36$ respectively in all cases, while in the spectrum for $x = 7D$, one dominant frequency $St = 0.09$ and several subpeaks with $0.1 < St < 0.4$ and almost the same amplitude are detected. The main frequency with the highest amplitude of the meandering for $4D$ downstream position corresponds to a period $T = D/(u_0 St) \approx 120s$, and this dominant frequency keeps the same value for $10D$ downstream position. But the subpeaks with relatively high frequency weaken as x increases and only the secondary peaks, of which the Strouhal number is between 0.1 ~ 0.3, remains remarkable until $x = 10D$, as illustrated in the last graph in Fig 10. The dominant low frequent meandering from $x = 4D$ to $x = 10D$ with a period up to 120s

is supposed to be affected by the kilometer scale flow structure in the atmospheric boundary layer, and the secondary frequency component of the wake meandering, with $0.1 < St < 0.3$, is also found in the experimental work by Okulov[21].

Conclusion

Performance optimization of a wind farm through yaw control is a realizable and promising technique but still needs a deep understanding of the wake characteristics of a yawed wind turbine operating in the atmospheric boundary layer. In the present work, the wake flow of a single wind turbine with and without a yaw angle is studied through actuator line model and LES technique. The velocity and turbulence intensity profiles of the flow generated in the precursor case show a typical stratification of a neutral boundary layer flow in the atmosphere and accord well with the prescribed wind velocity and direction.

For a turbine operating in yaw condition, the time-average velocity deficit is generally smaller than that of a non-yawed turbine, because the misalignment leads to the decrease of the effective wind speed, which is a function of the yaw angle γ. In the central longitudinal plane, the velocity deficit in far wake region behind a turbine with a yaw angle of $\pm 30°$ is much weaker than that behind a non-yawed turbine, indicating the power output of a turbine downwind could be raised significantly by yawing the turbines located upstream. Moreover, the profiles of the velocity deficit in all cases show self-similarity and obey well with the gaussian distribution in the horizontal plane. Nevertheless, through the contours of u_d in different cross sections downstream, the velocity distribution in the far wake of a yawed wind turbine is not symmetric but shows a kidney-shape and the direction of the vertical deflection of the wake center depends on the yaw direction, which reduces the accuracy of the analytical wake model based on the gaussian distribution assumption.

A filtering process proposed by Howard[22] is introduced to smear out the high frequent turbulence and highlight the wake meandering movement. The time history curves of the meandering for case 1~3 show high correlation, demonstrating that the large-scale movement of the wake follows the flow structure with the same scale in the incoming flow. The rms values of δ_μ for all cases increase as the wake flows downstream and show nearly the same magnitude until $x = 10D$. Furthermore, regardless of the yaw condition, the frequency spectrum analysis shows a constant dominant frequency in the far wake region, caused by the low frequent turbulence in the atmosphere and other subpeaks frequency components with $0.1 < St < 0.3$ are found from $4D$ to $10D$ downstream positions, which is a main factor that influences the fatigue loads of the wind turbines in a wind farm. Future work should focus on the wake meandering characteristics of wind turbines under different atmospheric stratifications and its influence on the performance and aerodynamic loads of downstream turbines.

Acknowledgements

This work is supported by the National Natural Science Foundation of China (51879159, 51490675, 11432009, 51579145), Chang Jiang Scholars Program (T2014099), Shanghai Excellent Academic Leaders Program (17XD1402300), Program for Professor of Special Appointment (Eastern Scholar) at Shanghai Institutions of Higher Learning (2013022), Innovative Special Project of Numerical Tank of Ministry of Industry and Information Technology of China (2016-23/09) and Lloyd's Register Foundation for doctoral student, to which the authors are most grateful.

Reference

[1] Fleming, P. A., Scholbrock, A. K., Jehu, A., Davoust, S., Osler, E., Wright, A. D., & Clifton, A. (2014). Field-test results using a nacelle-mounted lidar for improving wind turbine power capture by reducing yaw misalignment. In *Journal of Physics: Conference Series* (Vol. 524, No. 1, p. 012002). IOP Publishing.

[2] Fleming, P., Gebraad, P. M., Lee, S., van Wingerden, J. W., Johnson, K., Churchfield, M., ... & Moriarty, P. (2015). Simulation comparison of wake mitigation control strategies for a two-turbine case. *Wind Energy*, *18*(12), 2135-2143.

[3] Gebraad, P. M. O., Teeuwisse, F. W., Van Wingerden, J. W., Fleming, P. A., Ruben, S. D., Marden, J. R., & Pao, L. Y. (2016). Wind plant power optimization through yaw control using a parametric model for wake effects—a CFD simulation study. *Wind Energy*, *19*(1), 95-114.

[4] Grant, I., Parkin, P., & Wang, X. (1997). Optical vortex tracking studies of a horizontal axis wind turbine in yaw using laser-sheet, flow visualisation. *Experiments in fluids*, *23*(6), 513-519.

[5] Haans, W., van Kuik, G. A. M., & Van Bussel, G. J. W. (2007). Experimentally observed effects of yaw misalignment on the inflow in the rotor plane. In *Journal of Physics: Conference Series* (Vol. 75, No. 1, p. 012012). IOP Publishing.

[6] Krogstad, P. Å., & Adaramola, M. S. (2012). Performance and near wake measurements of a model horizontal axis wind turbine. *Wind Energy*, *15*(5), 743-756.

[7] Bartl, J. M. S., Mühle, F. V., Schottler, J., Sætran, L. R., Peinke, J., Adaramola, M. S., & Holling, M. (2018). Wind tunnel experiments on wind turbine wakes in yaw: effects of inflow turbulence and shear.

[8] Bastankhah, M., & Porté-Agel, F. (2015). A wind-tunnel investigation of wind-turbine wakes in yawed conditions. In *Journal of Physics: Conference Series* (Vol. 625, No. 1, p. 012014). IOP Publishing.

[9] Bastankhah, M., & Porté-Agel, F. (2016). Experimental and theoretical study of wind turbine wakes in yawed conditions. *Journal of Fluid Mechanics*, *806*, 506-541.

[10] Bastankhah, M., & Porté-Agel, F. (2019). Wind farm power optimization via yaw angle control: A wind tunnel study. *Journal of Renewable and Sustainable Energy*, *11*(2), 023301.

[11] Jiménez, Á., Crespo, A., & Migoya, E. (2010). Application of a LES technique to characterize the wake deflection of a wind turbine in yaw. *Wind energy*, *13*(6), 559-572.

[12] Vollmer, L., Steinfeld, G., Heinemann, D., & Kühn, M. (2016). Estimating the wake deflection downstream of a wind turbine in different atmospheric stabilities: an LES study. *Wind Energy Science*, *1*(2), 129-141.

[13] Qian, G. W., & Ishihara, T. (2018). A New Analytical Wake Model for Yawed Wind Turbines. *Energies*, *11*(3), 665.

[14] Sørensen, J. N., & Shen, W. Z. (2002). Numerical modeling of wind turbine wakes. Journal of fluids engineering, 124(2), 393-399.

[15] Mann, J. (1998). Wind field simulation. *Probabilistic engineering mechanics*, *13*(4), 269-282.

[16] Kraichnan, R. H. (1970). Diffusion by a random velocity field. *The physics of fluids*, *13*(1), 22-31.

[17] Troldborg, N., Sørensen, J. N., & Mikkelsen, R. F. (2009). Actuator line modeling of wind turbine wakes.

[18] Moeng, C. H. (1984). A large-eddy-simulation model for the study of planetary boundary-layer turbulence. Journal of the Atmospheric Sciences, 41(13), 2052-2062.

[19] Foti, D., Yang, X., Guala, M., & Sotiropoulos, F. (2016). Wake meandering statistics of a model wind turbine: Insights gained by large eddy simulations. Physical Review Fluids, 1(4), 044407.

[20] Larsen, G. C., Aagaard, H. M., Bingöl, F., Mann, J., Ott, S., Sørensen, J. N., ... & Larsen, T. J. (2007). Dynamic wake meandering modeling.

[21] Okulov, V. L., Naumov, I. V., Mikkelsen, R. F., Kabardin, I. K., & Sørensen, J. N. (2014). A regular Strouhal number for large-scale instability in the far wake of a rotor. *Journal of Fluid Mechanics*, *747*, 369-380.

[22] Howard, K. B., Singh, A., Sotiropoulos, F., & Guala, M. (2015). On the statistics of wind turbine wake meandering: An experimental investigation. Physics of Fluids, 27(7), 075103.